

CHEMISTRY

A European Journal

A Journal of



Accepted Article

Title: Cobalt oxide materials for the oxygen evolution catalysis via single-source precursor chemistry

Authors: Denis A. Kuznetsov, Dmitry Konev, Sergey Sokolov, and Ivan Fedyanin

This manuscript has been accepted after peer review and appears as an Accepted Article online prior to editing, proofing, and formal publication of the final Version of Record (VoR). This work is currently citable by using the Digital Object Identifier (DOI) given below. The VoR will be published online in Early View as soon as possible and may be different to this Accepted Article as a result of editing. Readers should obtain the VoR from the journal website shown below when it is published to ensure accuracy of information. The authors are responsible for the content of this Accepted Article.

To be cited as: *Chem. Eur. J.* 10.1002/chem.201802632

Link to VoR: <http://dx.doi.org/10.1002/chem.201802632>

Supported by
ACES

WILEY-VCH

FULL PAPER

Cobalt oxide materials for the oxygen evolution catalysis via single-source precursor chemistry

Denis A. Kuznetsov,^{*[a]} Dmitry V. Konev,^[a,b] Sergey A. Sokolov,^[c,d] Ivan V. Fedyanin,^[e]

Abstract: Utilization of the metal alkoxides as the single-source precursors for the (mixed-)oxide materials offers remarkable benefits such as possibility to precisely control the metal ratio in the resulting material, highly homogeneous distribution of the elements in the film and low temperatures required for films processing. Here we report on the isolation and characterization of the bimetallic Co-Mo alkoxide, $[\text{Co}_3\text{Mo}_4\text{O}_{10}(\text{OCH}_3)_{10}(\text{dmf})_4]$ (**Co₃Mo₄**) (dmf = N,N-dimethylformamide), which was prepared through the anion metathesis reaction from the corresponding metal chlorides. The latter was explored as a well-defined precursor for the oxides explored as the catalysts for the oxygen evolution reaction (OER). These catalysts demonstrate excellent activity in OER that manifests in low onset potentials and Tafel slopes and superb stability under operating conditions both in alkaline and nearly neutral media. It was observed that the nature of the metal cation of the alkaline electrolyte MOH ($\text{M}^+ = \text{Li}^+, \text{Na}^+, \text{K}^+, \text{Cs}^+$) greatly effects the catalytic performance of the material. We propose that the positive effect of the larger metal cations on the film activity in OER could be explained as a result of the higher hydration enthalpies of larger ions and better mass transport within larger interlayer space between $[\text{CoO}_2]^{2-}$ sheets of the *in situ* formed binary oxides. It may be deduced that this trend is universal and may be extended to the other types of metal oxides forming layered structures.

Introduction

Cost-effective conversion and storage of sunlight energy in form of energy of chemical bonds, which could be accomplished either directly - in the photoelectrocatalytic devices, or indirectly - in the

electrolyzers, is a cherished target for the whole scientific society as this potentially represents a long-awaited solution to a global demand for a renunciation of exhaustible fossil fuels. Valuable products (H_2 - for the case of water reduction; CO, methanol, hydrocarbons - for CO_2 reduction) are produced during the cathodic half-reaction, whereas an anodic process as a rule releases no value-added O_2 gas. The overall efficiency of such a device, however, is limited by the performance of both electrode components, and for the particular case of water splitting, OER overpotential limits to a considerable degree the overall efficiency of the electrochemical cell^[1,2]. Currently, the benchmark for the OER catalysts are Ru and Ir oxides, however low abundance of these metals precludes their large scale application. In this regard, non-noble metal catalysts, particularly those based on Ni(Fe)^[3] and Co^[4] oxo-hydroxides or perovskite oxides^[5,6] which demonstrate comparable or even superior performance compared to RuO_2 and IrO_2 , emerged as a promising option to replace the noble metal oxides in the state-of-the-art devices.

Apart from tuning the intrinsic activity of the catalyst, which is determined by its structure and composition, nanostructuring of the material could greatly contribute to its overall performance. Increase of the specific surface area could be achieved, for instance, by leaching or electrochemical dissolution of some of the bulk constituents^[7-11]. Following this argumentation, a synthetic protocol, which includes preparation of the multimetallic material whose certain constituents are then removed thus leaving porous, high surface area structure, could be devised^[12,13]. Heterometallic alkoxides seem to be an excellent option to accomplish this goal, as they are readily decomposable upon hydrolytic or thermal treatment producing homogeneous heterometallic oxides films whose element ratio is precisely defined by the precursor stoichiometry. Moreover, the potential for the tuning of the metal combinations is restricted only by inherent thermodynamic instability of particular metal-oxygen bonds, that makes alkoxide-precursor-based approach a universal means for production of the oxide coatings^[14-16], particularly for the energy applications^[13,17-22].

Another factor contributing to the efficiency of the electrolysis cell is the electrolyte species which, apart from the buffering role, can affect the catalyst performance through the structural tuning of the latter via cations or anions inclusion into the catalyst structure or via cation/anion effect on the interfacial water structure^[23,24]. Dependence of the OER activity on the electrolyte nature, particularly on the cation type^[25-28] is frequently observed. To explain this phenomenon, stabilization of the surface-bound anionic oxygen intermediates through the non-

[a] Dr. D. A. Kuznetsov, Dr. D. V. Konev
Institute of Problems of Chemical Physics, Russian Academy of Sciences, Chernogolovka, Moscow region, 142432, Russian Federation
E-mail: kuznetsov.denis.alex@gmail.com

[b] Dr. D. V. Konev
D. I. Mendeleev University of Chemical Technology of Russia, Moscow, 125047, Russian Federation

[c] S. A. Sokolov
Department of Chemistry, M. V. Lomonosov Moscow State University, Moscow, 119991, Russian Federation

[d] S. A. Sokolov
Institute of Nanotechnology of Microelectronics, Russian Academy of Sciences, Moscow, 119991, Russian Federation

[e] Dr. I. V. Fedyanin
A. N. Nesmeyanov Institute of Organoelement Compounds, Russian Academy of Sciences, Moscow, 119991, Russian Federation

Supporting information for this article is given via a link at the end of the document.

FULL PAPER

covalent interactions with counter-cations that might affect the reactivity of the surface^[27,28] is usually proposed. In this work, based on Pourbaix diagrams of cobalt and results of the energy-dispersive X-ray (EDX) spectroscopy, X-ray photoelectron spectroscopy (XPS) demonstrating that alkaline metal incorporates into the catalyst structure, we speculate that, in addition to the electronic effects discussed above^[27,28], improvement of activity can also be due to the lower hydration enthalpies of the larger alkaline cations and due to reduced mass transfer limitations in the larger $[\text{CoO}_2]^{6-}$ interlayer space for bigger cations in the binary oxides M^+CoO_2 *in situ* formed in M^+OH electrolyte. We may assume that this mechanism is also applicable for the other types of metal oxides which tend to form layered structure during OER.

Results and Discussion

Synthesis of the molecular precursor. Solid-state structure of $[\text{Co}_3\text{Mo}_4\text{O}_{10}(\text{OCH}_3)_{10}(\text{dmf})_4]$ (Co_3Mo_4)

Interest to molybdenum as a dopant for the cobalt- and nickel-based materials for water oxidation catalysis had arisen as a result of a number of reports describing high activity of the catalysts containing molybdenum as a counterpart to Ni, Co, Fe^[13,29–33]. This urged us to investigate compounds comprising these non-noble metals^[13] in combination with molybdenum to produce materials with high electrocatalytic activity towards water oxidation.

Complex $[\text{Co}_3\text{Mo}_4\text{O}_{10}(\text{OCH}_3)_{10}(\text{dmf})_4]$ (Co_3Mo_4) was prepared in a single step in the reaction of joint alcoholysis of CoCl_2 and MoO_2Cl_2 in the presence of the stoichiometric amounts of $\text{Mg}(\text{OCH}_3)_2$ at elevated temperature. As expected, thermal treatment caused formation of the oxo-groups (through the dialkylether elimination reaction^[34,35]) that eventually led to the isolation of a heptanuclear complex Co_3Mo_4 from the reaction mixture.

Planar centrosymmetric structure of Co_3Mo_4 comprised of seven edge-sharing octahedra is typical for oxo-compounds, particularly of cobalt and molybdenum^[36–39]. Three cobalt(II) and four molybdenum(VI) atoms are interconnected through the network of μ_2 - and μ_3 -methoxo- and oxo-bridges giving rise to a disc-like structure reminiscent to that of some bulk oxides (including the polymeric $\text{CoO}_x(\text{OH})_y$ sheets deduced to be the structural elements of CoPi OER catalysts developed by Nocera et al.^[38,40,41]). In this manuscript we will discuss the utilization of Co_3Mo_4 as a precursor for the single-step deposition of oxides on conducting substrates to catalyze OER.

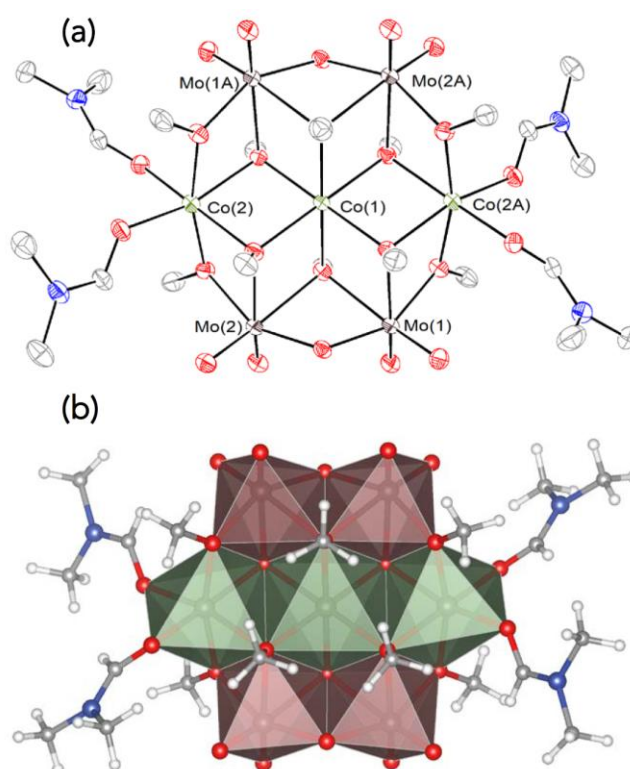


Figure 1. X-ray molecular structure of $[\text{Co}_3\text{Mo}_4\text{O}_{10}(\text{OCH}_3)_{10}(\text{dmf})_4]$ (Co_3Mo_4) as represented (a) by thermal ellipsoids and (b) by coordination polyhedra. Hydrogen atoms on (a) are omitted for clarity. Ellipsoids on (a) are drawn at 30 % probability level. Color code: Co – green; Mo – brown; O – red; N – blue; C – grey; H – white.

Thin film deposition and characterization

Polycondensation of metal-organic compounds, particularly metal alkoxides to form metal oxides could be performed under mild reaction conditions via sol-gel process^[15]. The first synthetic step represents hydrolysis of the metal alkoxides to produce sol/gel of hydrated metal oxides/hydroxides, which can then condense to form extended M-O-M chain of the nanoparticulate or bulk oxide phase through the dehydration or ether elimination reaction^[16]. Such single-source precursor (SSP) based approach offers notable advantages over conventional techniques, as the molecular precursor can in principle ensure the atomic level control over the product stoichiometry, elemental homogeneity in the resulting oxide nanostructure which can be tuned to meet the requirements of specific application. Overall, SSP approach has a great potential for the synthesis of the inorganic energy-related materials as it provides a tool for the precise control over material composition and surface properties via the fine tuning of the precursor structure and treatment conditions^[42]. In this and following section, we exemplify the advantages of the SSP-based

FULL PAPER

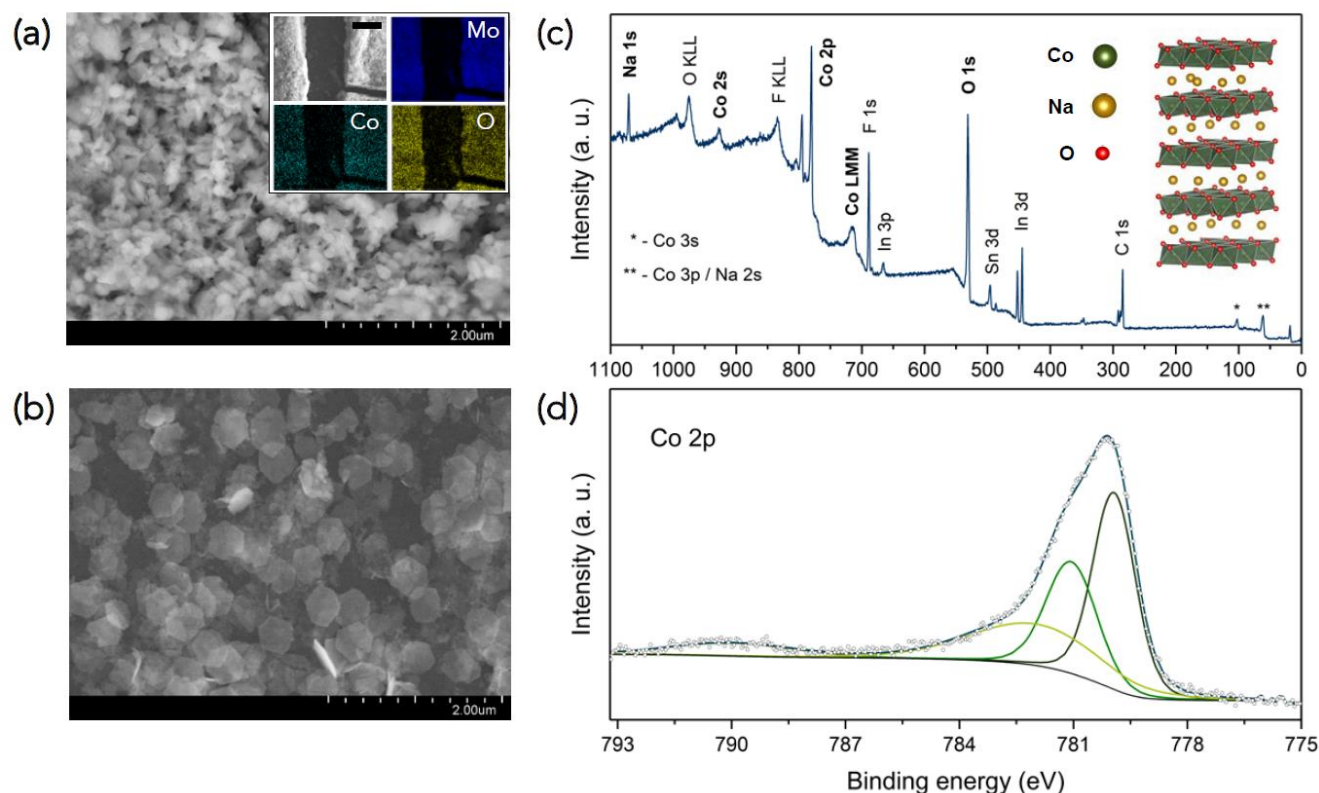


Figure 2. (a) SEM images of (a) as-deposited Co_3Mo_4 film and (b) Co_{cat} film. (c) Survey X-ray photoelectron (XPS) spectrum and (d) Co 2p region recorded for Co_{cat} film. Only the most intensive peaks corresponding to film constituents (Co, O, Na) are shown. Peaks corresponding to Sn, In are from ITO, and F is from Nafion binder. Carbon peak was set at 284.8 eV. Films for SEM imaging were deposited on glassy carbon substrate, for XPS measurements – on ITO coated glass substrate. Co_{cat} films were obtained by cycling and galvanostatic treatment of pristine material (see Experimental details). Inset on (c) shows schematic structure of the sodium salt of cobalt oxo-hydroxide $[(\text{CoOO})_x\text{Na}_y]$.

approach by demonstrating utilization of the alkoxide complex Co_3Mo_4 for the one-step preparation of the cobalt oxide-based films characterized by the high catalytic activity and remarkable stability in oxygen evolution (OER) reaction.

Electrodes for catalytic activity evaluation were initially prepared by drop-casting suspension of Co_3Mo_4 in isopropanol/water (+ Nafion binder) mixture onto pretreated^[43] glassy carbon surface. Screening of the electrochemical properties was performed in a conventional three-electrode setup in one molar alkaline electrolyte following recently suggested benchmarking protocol^[1,44,45]. Apart from electrochemical investigation, films were investigated by means of scanning electron microscopy (SEM), EDX and XPS measurements before and after electrochemical treatment.

Co_3Mo_4 precursor is deposited as a relatively flat film with a highly homogeneous distribution of elements and without any elemental impurities as confirmed by EDX and XPS analysis (see Figs. 2a, 2b). Before electrochemical testing, the film was preconditioned by cycling and galvanostatic treatment in the respective 1 M MOH electrolyte. As expected^[13], such treatment resulted in a complete removal of molybdenum from the film, that lead to formation of the material characterized by the enhanced surface area with estimated roughness factor 300 ± 120 (ratio of

the electrochemically active surface area of a given material to that of the atomically flat substrate). Interestingly, no notable increase of the ECSA was observed in the course of cycling, implying fast removal of Mo from the film (occurring presumably once the electrode is immersed in electrolyte). The importance of the presence of Mo in the precursor film can be highlighted by the comparison of Co catalyst (Co_{cat}) ECSA with that for various electrodeposited and cast films for which the reported ECSA values are typically of the order of tens^[1,45].

The Co $2p_{3/2}$ spectra of electrochemically treated film showed spectral features characteristic for the compound containing cobalt in the oxidation state Co^{3+} . The overall line shape or envelope in such Co $2p_{3/2}$ spectrum arises from multiplet splitting peaks with principle line 780.0 eV, analogous to previous XPS results^[46,47]. Absence of a peak in a region ca. 6 eV higher principle line, typical for multielectron excitation^[46,48], suggests Co^{3+} as the major oxidation state of cobalt in the sample, confirming that Co_3Mo_4 converts mostly to cobalt oxo-hydroxide $\text{CoO}_x(\text{OH})_{1-x}$ during electrochemical treatment.

The assignment of Co_{cat} as cobalt oxo-hydroxide is also indirectly confirmed by CV measurements. 2 sets of peaks on CV curves in a region 0.4 – 1.5 V vs. RHE (Fig. S3) correspond to $\text{Co}^{2+}/\text{Co}^{3+}$ and $\text{Co}^{3+}/\text{Co}^{4+}$ transitions^[49–51]. The oxidation at 1.1 V

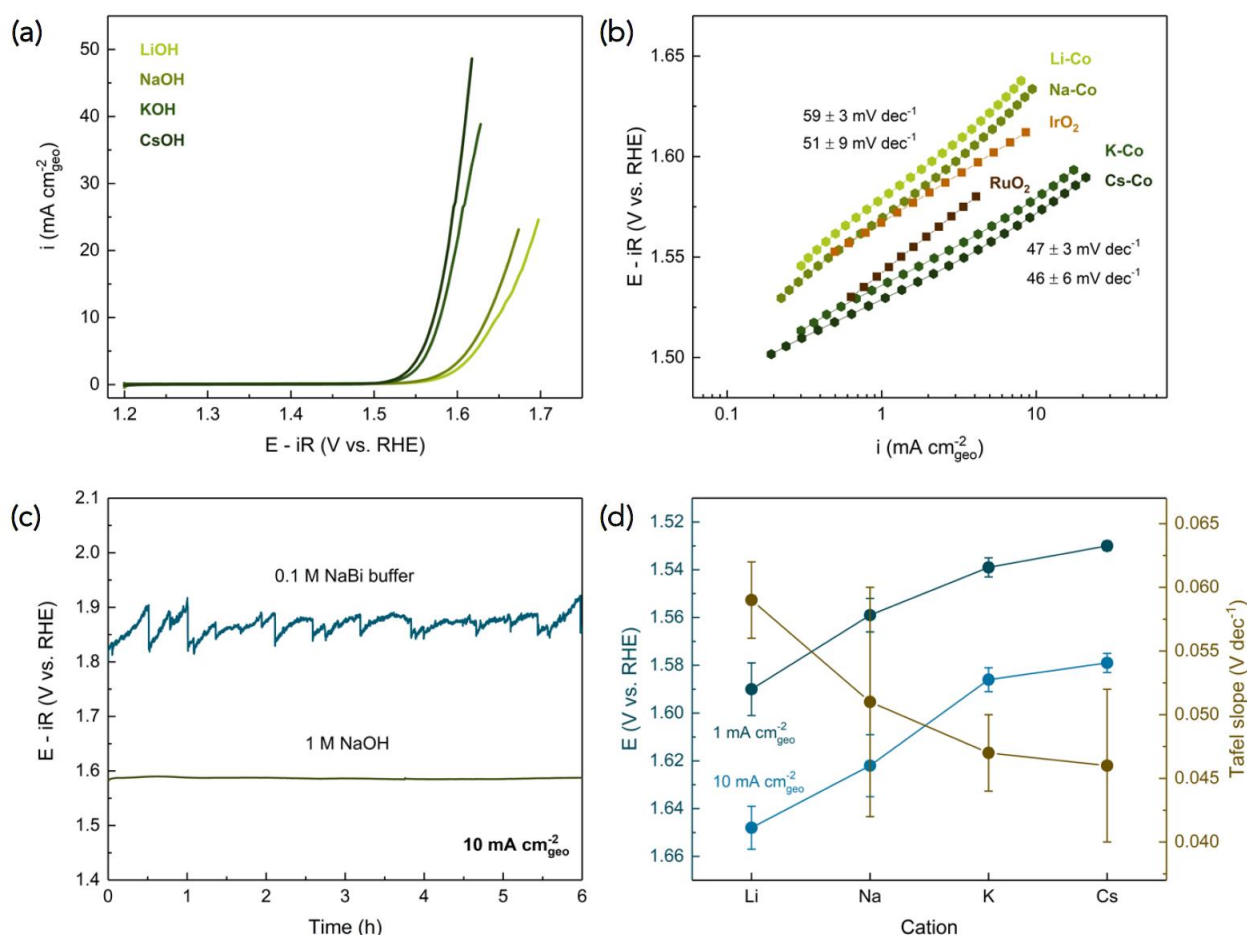


Figure 3. (a) Representative linear sweep voltammetry (LSV) curves and (b) derived Tafel plots recorded for Co_{cat} in different 1 M MOH electrolytes ($M = \text{Li}, \text{Na}, \text{K}, \text{Cs}$). The values of Tafel slopes are 59 ± 3 , 51 ± 9 , 47 ± 3 , 46 ± 6 mV decade^{-1} for Li^+ , Na^+ , K^+ , Cs^+ -intercalated species, respectively. Tafel plots for RuO_2 and IrO_2 (extracted from Ref. [45]) are given for comparison. (c) Galvanostatic curves recorded for Co_{cat} in 0.1 M sodium borate buffer (NaBi, pH 9.2) and 1 M NaOH. Electrodes were held at the constant current density of $10 \text{ mA cm}_{\text{geo}}^{-2}$. Catalyst films for galvanostatic measurements were deposited on pyrolytic carbon electrodes. (d) OER activity of Co_{cat} as represented by Tafel slopes and values of potentials to achieve current densities of 1 and $10 \text{ mA cm}_{\text{geo}}^{-2}$ as a function of the nature of MOH electrolyte cation ($M = \text{Li}, \text{Na}, \text{K}, \text{Cs}$). Data points represent average values extracted from LSV curves, error bars are standard deviations from at least 3 independent measurements.

vs. RHE results in a notable increase of the capacitance current assuming increase of the electrochemically active surface area (ECSA) after this redox event which can be accounted for the formation of the oxo-hydroxide phase comprised of oxide layers more accessible for electrolyte compared to hydroxide phase.

According to SEM, Co_{cat} films consist of 2 types of landscapes: domains with amorphous porous structure and regions comprised of the thin hexagonal plates (Fig. 2b, S1), similar to the reported observations for cobalt oxo-hydroxide species^[46]. Our data also clearly demonstrate the role of molybdenum in cobaltous films which was not explained in literature reporting on the investigation of transition metals (Ni, Co, Fe) molybdates for OER. Our study provides an evidence that dissolution of molybdenum upon reaction with alkaline electrolyte and potential cycling occurs, that results in formation of film with

high surface area, similar to the effect of chromium doping in Ni-Fe oxo-hydroxides^[7].

Effect of the alkaline metal cation and pH on OER activity

Electrocatalytic activity of Co_{cat} in oxygen evolution reaction (OER) was assessed through linear sweep voltammetry (LSV) measurements, and was demonstrated to possess remarkable pH and cation dependence. Figure 3 shows that OER activity of Co_{cat} strongly depends on the nature of M^+ cation when tested in 1 M MOH electrolyte ($M^+ = \text{Li}^+, \text{Na}^+, \text{K}^+, \text{Cs}^+$) where the activity increases in a row $\text{Li}^+ < \text{Na}^+ < \text{K}^+ \approx \text{Cs}^+$. Notably, the Tafel slopes also scale with cation size: 59 ± 3 , 51 ± 9 , 47 ± 3 , 46 ± 6 mV decade^{-1} for Li^+ , Na^+ , K^+ , Cs^+ -intercalated species, respectively, rendering the highest activity for K^+ and Cs^+ -intercalated oxides, reaching 10 mA cm^{-2} OER current density at the potential ca. 1.58

FULL PAPER

V vs. RHE, which is on par with noble metal RuO₂ and IrO₂ oxides (Fig. 3b, S5) and other state-of-the-art materials (Table S1).

The cation effect on activity was previously observed for different reactions including OER^[25–28,52–54], oxygen reduction reaction (ORR)^[23,55], CO reduction^[56] where dependence of activity on electrolyte nature is typically attributed to the difference in binding energies of the electrolyte cations with surface oxygen species and to the changes of the interfacial water structure. Here we propose that the evolution of the catalyst structure triggered by cation substitution may also be responsible for changes in activity.

From Pourbaix diagram of Co^[49] and from our XPS and EDX measurements, it clearly follows that under OER conditions, cobalt exists in form of layered [CoOO]^{δ-} species where counter-cations are located in the interlayer space. The increase of cation size results in a larger interlayer separation, which can benefit the mass transport of the substrates and products (water and oxygen) in the interlayer space, therefore effecting OER reaction kinetics. Similarly, the positive effect of the larger interlayer distance on the OER activity was recently demonstrated for model Mn-based catalyst, where layers separation strongly correlated with catalytic activity^[53]. Additionally, it was shown for another class of layered materials, MXenes, that the presence of cations in the interlayer space leads to decrease of the diffusion coefficient of water in M⁺-intercalated material^[57] presumably due to the formation of stable [M⁺(H₂O)_n] hydration complexes. Similarly, an analogous effect might be deduced to be responsible for the decreased activity of Co_{cat} in alkaline solutions comprising smaller cations, which are characterized with more negative hydration enthalpies^[58] and therefore form more stable hydrates. We should also note here that inductive effect^[59] from intercalated cations might also influence the activity.

Another notable feature of Co_{cat} is a pH-dependence of OER activity. Galvanostatic measurements represented on Fig. 3c clearly shows that OER activity of the film is substantially higher when tested under high pHs, as manifested in lower overpotentials required to achieve current density of 10 mA cm_{geo}⁻². Generally, the pH-dependent OER activity arises if the surface deprotonation is involved in either rate-limiting step or a chemical step preceding the rate limiting one^[60]. Such pH dependence is observed for many highly active OER catalysts, such as Ni-Fe oxo-hydroxides^[61], certain RuO₂ crystal orientations^[62], some perovskite oxides^[63].

Despite being lower at less alkaline pH, the OER activity and stability of Co_{cat} in nearly neutral media (borate buffer, pH 9.2) is remarkable, as the gradual loss of activity upon cycling in neutral media is a common phenomenon for many transition metal oxides^[64], whereas for Co_{cat} currents remain stable even after prolonged galvanostatic hold (fluctuations on E-t curve are due to intensive O₂ bubbles formation). Similarly high stability was also observed when Co_{cat} was tested in 1 M alkaline electrolytes, yielding 10 mA cm_{geo}⁻² OER current at 1.58 V vs. RHE under optimized conditions placing this material among the most active and stable OER catalysts, which clearly outperforms other reported molecular precursor-derived catalysts^[21,22,65–67].

High catalytic activity and stability makes Co_{cat} an attractive option for the practical utilization in electrocatalytic devices, as the

solution processed single-source precursor chemistry is an appealing approach for the preparing of the multifunctional coatings^[7] for conducting/semiconducting materials on a commercial scale, due to simplicity of the deposition procedure, its scalability and versatility of the potential precursors. In this respect, high OER activity maintained even at nearly neutral pH, is hugely beneficial as providing an opportunity for the use of Co_{cat} as the coating in photoelectrochemical cells utilizing natural water resources.

Conclusions

We have synthesized and fully characterized the novel bimetallic compound [Co₃Mo₄O₁₀(OCH₃)₁₀(dmf)₄] (Co₃Mo₄) (dmf = N,N-dimethylformamide). Well-defined molecular complex Co₃Mo₄ was drop-cast on conducting substrates to serve as a precursor for the oxide films which were obtained *in situ* during cycling of the electrodes in basic electrolytes at OER potentials. Molybdenum was shown to be removed from the bimetallic films providing high surface area films of cobalt oxo-hydroxides. These electrodes demonstrate very high OER activity which is a pH and cation-dependent. Both OER currents and Tafel slopes scale with the type of cation of the alkaline electrolyte where the lowest currents and highest Tafel slopes are characteristic for the films investigated in MOH electrolytes with smaller M⁺. Increase of activity upon transition from Li⁺ to Cs⁺ can be attributed to the weaker binding of the larger cations to the surface oxygen species and to a larger distance between [CoO₂]^{δ-} sheets of the catalyst and higher enthalpies of formation [M(H₂O)_n]⁺ hydrates enhancing water mobility in the interlayer space. The catalyst also demonstrates excellent activity in nearly neutral electrolyte (borate buffer, pH 9.2) making it a competing candidate for the use in the photoelectrocatalytic devices.

Experimental Section

Materials and reagents

All synthetic manipulations were carried out using standard Schlenk techniques under an argon atmosphere. Methanol and acetonitrile were dried upon refluxing with magnesium methoxide and CaH₂, respectively. Dimethylformamide (dmf) was distilled twice under reduced pressure. Solvents were stored over molecular sieves (4 Å for dmf, 3 Å for methanol and acetonitrile) under an argon atmosphere. Solution of Mg(OCH₃)₂ was prepared by the reaction of magnesium turnings with methanol. Commercially available MoO₂Cl₂ (Aldrich) was used as received. Anhydrous CoCl₂ was obtained by heating CoCl₂·6H₂O at 250°C *in vacuo* for 12 h. Solutions for electrochemical measurement were prepared from high purity LiOH, NaOH, KOH, CsOH.

Synthesis of [Co₃Mo₄O₁₀(OCH₃)₁₀(dmf)₄] (Co₃Mo₄) and X-ray structure characterization

CoCl₂ (1.0 mmol) solution in methanol (2 ml) and MoO₂Cl₂ (1.0 mmol) solution in methanol (5 ml) were consequently added to a Schlenk flask. To this mixture, Mg(OCH₃)₂ (2.0 mmol) in methanol (3 ml) was added. Deep-red solution obtained was refluxed for 30 min and then left stirred

FULL PAPER

overnight at room temperature. Solution was decanted from pink crystalline precipitate and the latter was washed with methanol (2 + 2 ml). To this wet pink residue (vacuum drying results in formation of unreactive blue solid), acetonitrile (2 ml) and dmf (1 ml) were added producing bright blue solution from which large pink prismatic crystals precipitated in a course of 1 week (ca. 0.5 ml CH₃OH should be added to this solution if precipitation is not observed). Crystals were washed with methanol (2 + 2 ml) and gently dried affording Co₃Mo₄ in 5-10% yield. IR (cm⁻¹): 2941 w, 2827 w, 1658 s, 1500 w, 1437 w, 1419 w, 1384 m, 1254 w, 1113 w, 1045 m, 1011 s, 931 s, 903 vs, 894 s, 681 vs. Calc. for C₂₂H₅₈O₂₄N₄Mo₄Co₃, (%): C, 19.97; H, 4.42; N, 4.23. Found, (%): C, 20.52; H, 4.76; N, 4.19.

X-ray diffraction data for Co₃Mo₄ were collected on a Bruker APEX DUO diffractometer ($\lambda(\text{CuK}\alpha) = 1.54178 \text{ \AA}$, $2\theta < 141.97^\circ$, φ and ω scans with 0.6° scan step and 4 to 8 s per frame exposure). Pink crystals of C₂₂H₅₈O₂₄N₄Mo₄Co₃ at 120(2) K are monoclinic, space group P21/c, $a = 8.0813(4)$, $b = 14.6514(5)$, $c = 18.4954(6)$ Å, $\beta = 96.478(2)^\circ$, $V = 2175.92(15) \text{ \AA}^3$, $Z = 2$, $d_{\text{calc}} = 2.020 \text{ g cm}^{-3}$. The indexing revealed that the structure was twinned. Frames were integrated by a narrow-frame algorithm using SAINT software package^[68], both twin domains were included in the integration. Semi-empirical absorption correction was applied with TWINABS^[69] program using intensity data for equivalent reflections. Intensities of 4206 independent reflections ($R_{\text{int}} = 0.0918$) out of 46394 collected were used in structure solution and refinement. The structure was solved by direct methods and refined by the full-matrix least-squares technique against F^2 in the anisotropic-isotropic approximation. The positions of hydrogen atoms were calculated. Hydrogen atoms were refined in riding model with $U_{\text{iso}}(\text{H})$ equal to $1.5 U_{\text{eq}}(\text{C})$ and $1.2 U_{\text{eq}}(\text{C})$ of the connected methyl and other carbon atoms. The refinement converged to $R1 = 0.0534$ (calculated for 3915 observed reflections with $I > 2\sigma(I)$), $wR2 = 0.1551$ and $\text{GOF} = 1.073$. The refinement calculations was performed with SHELX software package^[61]. Atomic coordinates, bond lengths and angles and thermal parameters have been deposited at the Cambridge Crystallographic Data Center, CCDC number 1534944.

Instrumentation

The infrared spectra were measured on solid samples using a Perkin Elmer Spectrum 100 Fourier Transform infrared spectrometer.

Electron microscopy images were recorded using either FEI Nova NanoSEM 230 with a field emission source and adjustment of the accelerating voltage up to 30 kV with a precision step of 0.1 kV coupled with an energy dispersive x-ray detector Bruker XFlash 5010 or Hitachi SU8000 field-emission scanning electron microscope equipped with Oxford Instruments X-Max EDX detector. Images were acquired in a secondary electron mode with accelerating voltages 2 - 15 kV.

X-ray photoelectron spectroscopy (XPS) of the as-deposited Co₃Mo₄ and the catalyst films obtained upon preconditioning of the as-deposited Co₃Mo₄ (treatment with corresponding base, potential cycling and 60 min electrolysis in 1 M alkaline solution at 2 mA cm^{-2}) were carried out using a KRATOS AXIS ULTRA DLD spectrometer (Kratos Analytical Ltd., United Kingdom). The probed area for each sample was $300 \times 700 \mu\text{m}^2$, and the probing depth was 1–2 nm. Monochromatic X-rays were generated by an Al K α source (1486.6 eV), energy resolution 0.6 eV. Binding energies of XPS spectra were calibrated against the C 1s peak of the adventitious carbon (284.8 eV) as an internal standard.

AFM images were obtained using an NTEGRA PRIMA instrument (NT-MDT, Russia).

All electrochemical measurements were carried out at room temperature using Autolab PGSTAT 302 N or Elnis P-45X potentiostats controlled by Nova or ES8 software, respectively, in a single-compartment cell using conventional three-electrode setup. Co₃Mo₄-derived thin film-coated glassy carbon (GC), pyrolytic carbon (PC) and ITO-coated glass electrodes were prepared, as described below, and used as working electrodes. Saturated silver chloride Ag/AgCl, KCl(sat.) [$E_{\text{Ag/AgCl, KCl(sat.)}} = 0.197 \text{ V vs. NHE}$] electrode was used as a reference electrode and a platinum mesh was employed as a counter electrode. Potentials are reported against RHE, recalculations were performed using the Nernst equation: $E(\text{V vs. RHE}) = E(\text{V vs. Ag/AgCl, KCl(sat.)}) + 0.197 + (0.059 \times \text{pH})$. Cyclic voltammetry (CV) and linear sweep voltammetry (LSV) measurements were automatically corrected for IR drop using Nova or ES8 software. Chronopotentiometric measurements were manually corrected for IR drop. Electrical Impedance Spectroscopy (EIS) was used to determine R value which was typically in the range 7–14 Ohm for 1 M alkaline electrolyte solutions and 140–160 Ohm for 0.1 M sodium borate solutions. Electrochemical capacitance was determined using CV measurements in a potential range where there is a non-Faradaic current response (on a plateau between Co^{2+/3+} and Co^{3+/4+} waves: 1.2 – 1.3 V vs RHE).

Electrode preparation

Glassy carbon (GC) electrodes (Sigradur® G) with a diameter of 3 mm or pyrolytic carbon (PC) electrodes (Volta) with a diameter of 3 mm were polished consequently with alpha alumina powders of decreasing size suspended in distilled water. After each polishing step, the electrodes were thoroughly rinsed with bidistilled water. Then the electrodes were ultrasonicated consequently in bidistilled water and absolute ethanol for 10 seconds each, and dried with compressed air. Subsequently, the polished GC electrodes were pretreated electrochemically as described in ref.^[43]. The bare working electrode underwent 20 CV cycles at a potential window of 0.5 to 1.9 V vs. RHE at a scan rate of 100 mV s^{-1} in 1 M NaOH or KOH. Finally, the pretreated electrode was rinsed with absolute ethanol and dried with compressed air. No electrochemical pretreatment was performed for the PC electrodes. Before deposition, Co₃Mo₄ (8 mg) was suspended in 1 ml of H₂O + isopropanol mixture (3:1 v/v) to which 20 μL of Nafion (10 %) binder was added. Upon 30 min of sonication, 15 μL of the Co₃Mo₄ suspension was drop-cast portionwise onto electrode surface using microsyringe, and the solvent was allowed to evaporate in air. The catalyst loadings were 1.70 mg cm^{-2} (0.36 mg cm^{-2} based on active mass in form of cobalt(II) hydroxide Co(OH)₂). Dried film was then covered with drop of 1 M alkaline solution and was left to dry overnight in air. ITO-coated glass (Lumtec, resistance $4\text{--}6 \Omega \text{ sq}^{-1}$, 0.7 mm thickness) sheets ($2.5 \times 7.5 \text{ cm}^2$) were cut into $2.5 \times 0.5 \text{ cm}^2$ slides and were cleaned by consequent ultrasonication in acetone, bidistilled water and finally in isopropanol for 5 min each. Electrodes were fabricated by drop casting the Co₃Mo₄ suspension as described previously^[13]; catalyst loadings were the same as for GC and PC electrodes. Before SEM/EDX and XPS measurements electrodes were pretreated by cycling in 1 M alkaline solution until the currents stabilize and were then held at 2 mA cm^{-2} for 60 min.

The mean values of Tafel slopes and potentials to achieve the current density of 1 mA cm^{-2} or 10 mA cm^{-2} (Fig. 3d) represent average values extracted from LSV curves (Fig. S4), error bars are standard deviations from at least 3 independent measurements.

Acknowledgements

The work was supported by the Russian Foundation for Basic Research (grant № 16-33-00754 mol_a). The authors are grateful

FULL PAPER

to Dr. Igor V. Chistyakov (Zelinsky Institute of Organic Chemistry, Russian Academy of Sciences) for the preliminary SEM/EDX studies of some cobaltous films and to Rais N. Mozhchil and Dr. Andrey M. Ionov (Institute of Solid State Physics, Russian Academy of Sciences) for performing XPS measurements.

Keywords: water splitting • oxygen evolution reaction • cobalt • precursor • alkoxide

- [1] C. C. L. McCrory, S. Jung, I. M. Ferrer, S. M. Chatman, J. C. Peters, T. F. Jaramillo, *J. Am. Chem. Soc.* **2015**, *137*, 4347–4357.
- [2] N.-T. Suen, S.-F. Hung, Q. Quan, N. Zhang, Y.-J. Xu, H. M. Chen, *Chem. Soc. Rev.* **2017**, *46*, 337–365.
- [3] F. Dionigi, P. Strasser, *Adv. Energy Mater.* **2016**, *6*, 1600621.
- [4] J. Wang, W. Cui, Q. Liu, Z. Xing, A. M. Asiri, X. Sun, *Adv. Mater.* **2015**, *28*, 215–230.
- [5] J. Suntivich, K. J. May, H. A. Gasteiger, J. B. Goodenough, Y. Shao-Horn, *Science* **2011**, *334*, 1383–1385.
- [6] A. Grimaud, K. J. May, C. E. Carlton, Y.-L. Lee, M. Risch, W. T. Hong, J. Zhou, Y. Shao-Horn, *Nat. Commun.* **2013**, *4*, 2439.
- [7] D. Xu, M. B. Stevens, Y. Rui, G. DeLuca, S. W. Boettcher, E. Reichmanis, Y. Li, Q. Zhang, H. Wang, *Electrochimica Acta* **2018**, *265*, 10–18.
- [8] F. Song, K. Schenk, X. Hu, *Energy Environ. Sci.* **2016**, *9*, 473–477.
- [9] J. Rosen, G. S. Hutchings, F. Jiao, *J. Am. Chem. Soc.* **2013**, *135*, 4516–4521.
- [10] L.-K. Wu, J.-M. Hu, J.-Q. Zhang, C.-N. Cao, *J. Mater. Chem. A* **2013**, *1*, 12885–12892.
- [11] H. Tüysüz, Y. J. Hwang, S. B. Khan, A. M. Asiri, P. Yang, *Nano Res.* **2013**, *6*, 47–54.
- [12] D. Lei, J. Benson, A. Magasinski, G. Berdichevsky, G. Yushin, *Science* **2017**, *355*, 267.
- [13] D. A. Kuznetsov, D. V. Konev, N. S. Komarova, A. M. Ionov, R. N. Mozhchil, I. V. Fedyanin, *Chem. Commun.* **2016**, *52*, 9255–9258.
- [14] V. G. Kessler, *Chem. Commun.* **2003**, 1213–1222.
- [15] G. A. Seisenbaeva, V. G. Kessler, *Nanoscale* **2014**, *6*, 6229–6244.
- [16] N. Y. Turova, E. P. Turevskaya, V. G. Kessler, M. I. Yanovskaya, *The Chemistry of Metal Alkoxides*, Springer US, **2002**.
- [17] M. Crespo-Quesada, E. Reisner, *Energy Environ. Sci.* **2017**, *10*, 1116–1127.
- [16] Y.-H. Lai, D. W. Palm, E. Reisner, *Adv. Energy Mater.* **2015**, *5*, 1501668.
- [17] Y.-H. Lai, H. S. Park, J. Z. Zhang, P. D. Matthews, D. S. Wright, E. Reisner, *Chem. – Eur. J.* **2015**, *21*, 3919–3923.
- [20] Y.-H. Lai, M. Kato, D. Mersch, E. Reisner, *Faraday Discuss.* **2014**, *176*, 199–211.
- [19] Y.-H. Lai, T. C. King, D. S. Wright, E. Reisner, *Chem. – Eur. J.* **2013**, *19*, 12943–12947.
- [22] Y.-H. Lai, C.-Y. Lin, Y. Lv, T. C. King, A. Steiner, N. M. Muresan, L. Gan, D. S. Wright, E. Reisner, *Chem. Commun.* **2013**, *49*, 4331–4333.
- [23] D. Strmcnik, K. Kodama, D. van der Vliet, J. Greeley, V. R. Stamenkovic, N. M. Marković, *Nat. Chem.* **2009**, *1*, 466.
- [24] S. Nihonyanagi, S. Yamaguchi, T. Tahara, *J. Am. Chem. Soc.* **2014**, *136*, 6155–6158.
- [25] V. Colic, M. D. Pohl, D. Scieszka, A. S. Bandarenka, *Electrocatalysis* **2016**, *262*, 24–35.
- [26] J. D. Michael, E. L. Demeter, S. M. Illes, Q. Fan, J. R. Boes, J. R. Kitchin, *J. Phys. Chem. C* **2015**, *119*, 11475–11481.
- [27] J. Suntivich, E. E. Perry, H. A. Gasteiger, Y. Shao-Horn, *Electrocatalysis* **2013**, *4*, 49–55.
- [28] P. Hosseini-Benhangi, M. A. Garcia-Contreras, A. Alfantazi, E. L. Gyenge, *J. Electrochem. Soc.* **2015**, *162*, F1356–F1366.
- [29] M. Q. Yu, L. X. Jiang, H. G. Yang, *Chem. Commun.* **2015**, *51*, 14361–14364.
- [30] M. Kumar, R. Awasthi, A. S. K. Sinha, R. N. Singh, *Int. J. Hydrog. Energy* **2011**, *36*, 8831–8838.
- [31] J. Tian, N. Cheng, Q. Liu, X. Sun, Y. He, A. M. Asiri, *J. Mater. Chem. A* **2015**, *3*, 20056–20059.
- [32] R. N. Singh, Madhu, R. Awasthi, S. K. Tiwari, *Int. J. Hydrog. Energy* **2009**, *34*, 4693–4700.
- [33] V. K. V. P. Srirapu, C. S. Sharma, R. Awasthi, R. N. Singh, A. S. K. Sinha, *Phys. Chem. Chem. Phys.* **2014**, *16*, 7385–7393.
- [34] V. G. Kessler, K. V. Nikitin, A. I. Belokon, *Polyhedron* **1998**, *17*, 2309–2311.
- [35] N. Y. Turova, V. G. Kessler, S. I. Kucheiko, *Polyhedron* **1991**, *10*, 2617–2628.
- [36] S. T. Meally, C. McDonald, P. Kealy, S. M. Taylor, E. K. Brechin, L. F. Jones, *Dalton Trans.* **2012**, *41*, 5610–5616.
- [37] M. Moragues-Canovás, C. E. Talbot-Eeckelaers, L. Catala, F. Lloret, W. Wernsdorfer, E. K. Brechin, T. Mallah, *Inorg. Chem.* **2006**, *45*, 7038–7040.
- [38] A. M. Ullman, D. G. Nocera, *J. Am. Chem. Soc.* **2013**, *135*, 15053–15061.
- [39] Y.-L. Zhou, M.-H. Zeng, L.-Q. Wei, B.-W. Li, M. Kurmoo, *Chem. Mater.* **2010**, *22*, 4295–4303.
- [40] M. W. Kanan, D. G. Nocera, *Science* **2008**, *321*, 1072–1075.
- [41] Y. Surendranath, M. W. Kanan, D. G. Nocera, *J. Am. Chem. Soc.* **2010**, *132*, 16501–16509.
- [44] M. Driess, C. Panda, P. W. Menezes, *Angew. Chem. Int. Ed.* **2018**, DOI: 10.1002/anie.201803673.
- [43] L.-A. Stern, X. Hu, *Faraday Discuss.* **2014**, *176*, 363–379.
- [44] C. C. L. McCrory, S. Jung, J. C. Peters, T. F. Jaramillo, *J. Am. Chem. Soc.* **2013**, *135*, 16977–16987.
- [45] S. Jung, C. C. L. McCrory, I. M. Ferrer, J. C. Peters, T. F. Jaramillo, *J. Mater. Chem. A* **2016**, *4*, 3068–3076.
- [46] J. Yang, H. Liu, W. N. Martens, R. L. Frost, *J. Phys. Chem. C* **2010**, *114*, 111–119.
- [47] Z. Chen, C. X. Kronawitter, Y.-W. Yeh, X. Yang, P. Zhao, N. Yao, B. E. Koel, *J. Mater. Chem. A* **2017**, *5*, 842–850.
- [48] N. S. McIntyre, M. G. Cook, *Anal. Chem.* **1975**, *47*, 2208–2213.
- [49] J. B. Gerken, J. G. McAlpin, J. Y. C. Chen, M. L. Rigsby, W. H. Casey, R. D. Britt, S. S. Stahl, *J. Am. Chem. Soc.* **2011**, *133*, 14431–14442.
- [50] R. L. Doyle, I. J. Godwin, M. P. Brandon, M. E. G. Lyons, *Phys. Chem. Chem. Phys.* **2013**, *15*, 13737–13783.
- [51] L. D. Burke, M. E. Lyons, O. J. Murphy, *J. Electroanal. Chem.* **1982**, *132*, 247–261.
- [52] J. Zaffran, M. B. Stevens, C. D. M. Trang, M. Nagli, M. Shehadeh, S. W. Boettcher, M. Caspary Toroker, *Chem. Mater.* **2017**, *29*, 4761–4767.
- [53] Q. Kang, L. Vernisse, R. C. Remsing, A. C. Thenuwara, S. L. Shumlas, I. G. McKendry, M. L. Klein, E. Borguet, M. J. Zdilla, D. R. Strongin, *J. Am. Chem. Soc.* **2017**, *139*, 1863–1870.
- [54] Q. Gao, C. Ranjan, Z. Pavlovic, R. Blume, R. Schlögl, *ACS Catal.* **2015**, *5*, 7265–7275.
- [55] D. Strmcnik, D. F. van der Vliet, K.-C. Chang, V. Komanicky, K. Kodama, H. You, V. R. Stamenkovic, N. M. Marković, *J. Phys. Chem. Lett.* **2011**, *2*, 2733–2736.
- [56] E. Pérez-Gallent, G. Marcandalli, M. C. Figueiredo, F. Calle-Vallejo, M. T. M. Koper, *J. Am. Chem. Soc.* **2017**, *139*, 16412–16419.
- [57] N. C. Osti, M. Naguib, A. Ostadhossein, Y. Xie, P. R. C. Kent, B. Dyatkin, G. Rother, W. T. Heller, A. C. T. van Duin, Y. Gogotsi, et al., *ACS Appl. Mater. Interfaces* **2016**, *8*, 8859–8863.
- [58] J. Mähler, I. Persson, *Inorg. Chem.* **2012**, *51*, 425–438.
- [59] D. A. Kuznetsov, B. Han, Y. Yu, R. R. Rao, J. Hwang, Y. Román-Leshkov, Y. Shao-Horn, *Joule* **2018**, *2*, 225–244.
- [60] L. Giordano, B. Han, M. Risch, W. T. Hong, R. R. Rao, K. A. Stoerzinger, Y. Shao-Horn, *Catal. Today* **2016**, *262*, 2–10.
- [61] M. Görlin, J. Ferreira de Araújo, H. Schmies, D. Bernsmeier, S. Dresch, M. Gliech, Z. Jusys, P. Cherev, R. Kraehnert, H. Dau, et al., *J. Am. Chem. Soc.* **2017**, *139*, 2070–2082.

FULL PAPER

- [62] K. A. Stoerzinger, R. R. Rao, X. R. Wang, W. T. Hong, C. M. Rouleau, Y. Shao-Horn, *Chem* **2017**, *2*, 668–675.
- [63] A. Grimaud, O. Diaz-Morales, B. Han, W. T. Hong, Y.-L. Lee, L. Giordano, K. A. Stoerzinger, M. T. M. Koper, Y. Shao-Horn, *Nat. Chem.* **2017**, *9*, 457–465.
- [64] B. Han, M. Risch, Y.-L. Lee, C. Ling, H. Jia, Y. Shao-Horn, *Phys. Chem. Chem. Phys.* **2015**, *17*, 22576–22580.
- [65] S. Suseno, C. C. L. McCrory, R. Tran, S. Gul, J. Yano, T. Agapie, *Chem. – Eur. J.* **2015**, *21*, 13420–13430.
- [66] A. Singh, S. L. Y. Chang, R. K. Hocking, U. Bach, L. Spiccia, *Energy Environ. Sci.* **2013**, *6*, 579–586.
- [67] X. Li, E. B. Clatworthy, A. F. Masters, T. Maschmeyer, *Chem. – Eur. J.* **2015**, *21*, 16578–16584.
- [68] SAINT v8.34A., Bruker AXS, Madison, Wisconsin, USA, **2013**.
- [69] G. M. Sheldrick, TWINABS V2008/4, Bruker AXS, Madison, Wisconsin, USA, **2008**.
- [70] G. M. Sheldrick, *Acta Crystallogr. Sect. C* **2015**, *71*, 3–8.